PHYSICAL REVIEW E **80**, 055401(R) (2009)

Numerical simulation of harmonic generation by relativistic laser interaction with a grating

X. Lavocat-Dubuis and J.-P. Matte
INRS-Énergie, Matériaux et Télécommunications, Varennes, Québec, Canada J3X 1S2

(Received 28 October 2008; revised manuscript received 9 October 2009; published 10 November 2009)

The interaction of a femtosecond relativistic intensity laser pulse with a grating of subwavelength periodicity was simulated numerically. Strong coherent emission at the wavelength of the grating period and its harmonics was seen, nearly parallel to the target surface, due to relativistic electron bunches emanating from each protuberance. Normal and oblique incidence (30°) gave rise to trains of attosecond pulses and an efficiency greater than 10^{-4} was obtained for the 24th harmonic ($\lambda \simeq 16.7$ nm). Similarity theory gives optimum conditions for harmonic emission.

DOI: 10.1103/PhysRevE.80.055401 PACS number(s): 52.38.Dx, 42.65.Ky, 52.35.Mw, 52.65.Rr

Laser technology now makes it possible to generate extremely short (12 fs) and intense ($>10^{22}$ W/cm^2) pulses [1,2]. The relativistic interaction of such pulses with matter introduces new phenomena such as hole boring, relativistic particle acceleration [1], and the creation of highly energetic electron bunches [3]. It is also a source of ultrashort x-ray emission, by line radiation [4], as well as high-order harmonics generation due to the electrons' highly nonlinear motion, which was studied experimentally, numerically, and analytically [1,5–9]. Short duration x-ray and extreme ultraviolet (XUV) sources have many applications in probing fast processes in matter [1].

When an intense femtosecond pulse is focused on a target, matter is ionized and heated almost immediately before the plasma can expand. Therefore, the interaction is with a solid density plasma and reflection is almost total due to the high plasma conductivity. Nanostructuring the target surface has been shown to considerably enhance absorption at moderate intensity, making the plasma hotter and hence a stronger emitter of x-ray radiation [4,10]. When resonant excitation of surface plasmons occurs, the absorption is almost complete [11], further enhancing the x-ray yield. When the laser intensity exceeds 10^{16} W/cm^2, charge separation needs to be taken into account, and it causes strong transverse and longitudinal electrostatic fields on the surface of a grating target which efficiently heat electrons [12]. At higher intensity, energetic electron bunches are formed due to acceleration by surface plasmon fields [13] when a sinusoidal surface plasma modulation of near wavelength periodicity is introduced, and relativistic effects can induce a saturation of these fields' amplitude, altering the plasmon resonance [14].

Here, we present the first study of harmonic emission due to the interaction of a relativistic intensity ($I_L > 10^{20}$ W/cm^2) and ultrashort ($\tau_L \sim 10$ fs) laser pulse with a grating surface having a periodicity a considerably less than the laser wavelength λ_L ($a/\lambda_L = 1/4$). This precludes resonant surface plasmon excitation which require a near wavelength periodicity $2/3 \leq a/\lambda_L \leq 1$ [11,13].

We show that, at each grating protuberance, relativistic electron bunches are generated, which lead not only to high laser energy absorption, but also to the emission of intense and coherent harmonics of the grating periodicity along the grating surface, i.e., at a grazing angle. The emitted fields come out as attosecond pulse trains which may have applications in studying the electron dynamics of matter [1]. We also show that the similarity parameter defined by Gordienko *et al.* for smooth targets [15,16], $S = N_e/(a_0 N_c)(\propto N_e \lambda_L / I_L^{1/2})$, is also relevant for corrugated ones: the conversion efficiency is fairly constant if S is held fixed. Here $a_0 = P_{osc}/(m_e c) = eE_L/(m_e \omega_L c)$ is the normalized quiver momentum of an electron in the laser field E_L, N_e is the electron density, $N_c = m_e \epsilon_0 \omega_L^2 / e^2$ is the critical density, and $\omega_L = 2\pi c/\lambda_L$.

The study was carried out with the $2\frac{1}{2}$ dimensional (x, y, P_x, P_y, P_z) relativistic and electromagnetic particle in cell (PIC) code XOOPIC [17]. The incident laser wavelength $\lambda_L = 400$ nm is the second harmonic of the Ti:sapphire laser, but the results can be easily rescaled for other laser wavelengths. The plasma was $8\lambda_L$ wide and λ_L thick. The simulation box was $15\lambda_L$ wide and $10\lambda_L$ long and the cell size was $\lambda_L/160$. The grating periodicity was set to $a = \lambda_L/4$, the height of the protuberances to $h = \lambda_L/8$ and their width to $e = \lambda_L/16$. The plasma density was initially $N_e = 20N_c = 1.4 \times 10^{23}$ cm^{-3}. The laser pulse was Gaussian in time (10 fs) and across the 3 μm spot size. The laser intensity was $I_L = I_{std} = 2 \times 10^{20}$ W/cm^2 ($S \simeq 4$). The electrons were represented by 20×10^6 superparticles. The ions were assumed immobile: comparating mobile and immobile ions runs with a longer pulse ($\tau_L = 20$ fs instead of 10 fs) with a realistic mass ratio (1836) showed little difference.

The geometry of the laser-plasma interaction is illustrated on Fig. 1. The laser was p polarized and incident at an angle θ_i. The spectra and the angular distributions of the harmonics were obtained by recording, at each time step, the magnetic field component B_z along a circle centered at the plasma

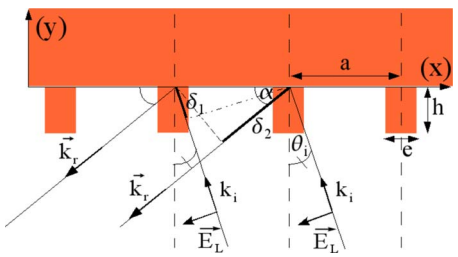

FIG. 1. (Color online) Interaction geometry. The laser beam is incident at an angle θ_i from the normal of the plasma surface and α is the direction of observation. $\delta_1, \delta_2, a, h, e$ are the phase differences between the incident rays and reflected rays, the grating periodicity, the height and width of the protuberances, respectively.

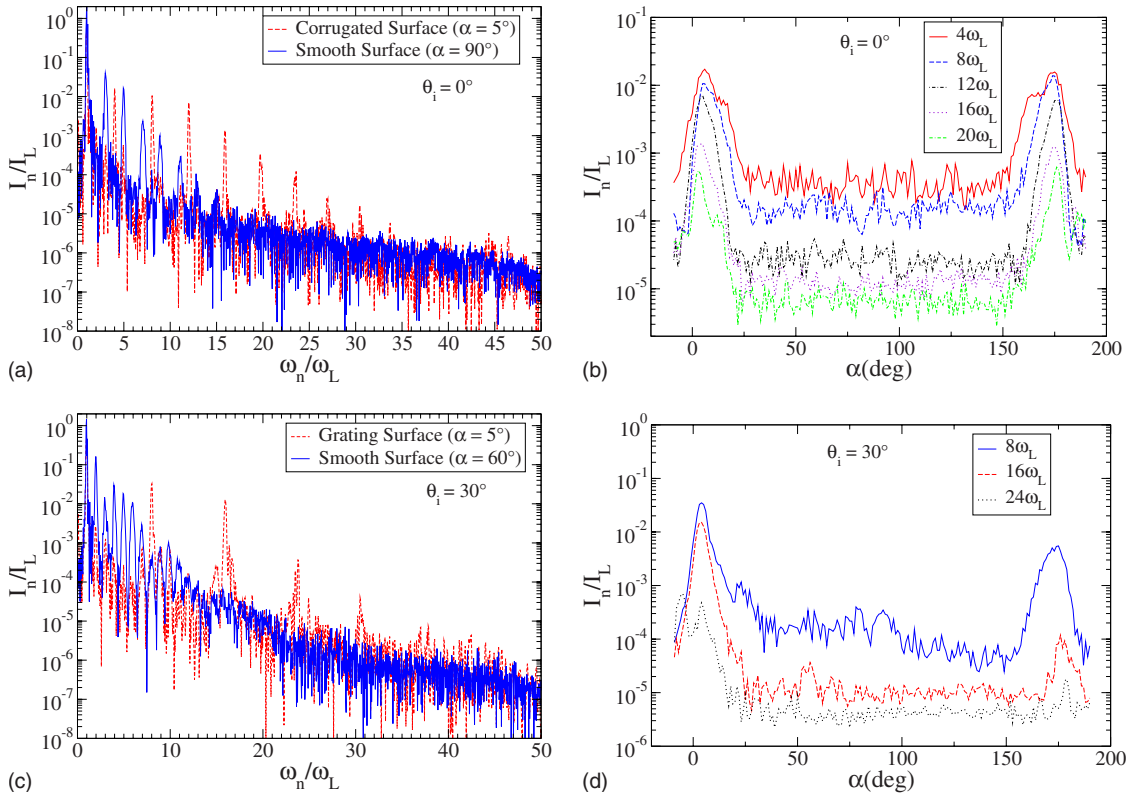

FIG. 2. (Color online) Spectrum at near grazing angle (α=5°) for grating surfaces and at [(a) and (c)] the specular angle (α=90 and 60°) for smooth surfaces and [(b) and (d)] angular distribution of several harmonics for grating surfaces at [(a) and (b)] normal incidence (θ_i=0°) and [(c) and (d)] oblique incidence (θ_i=30°).

surface and passing $\lambda_L/8$ from the edges of the simulation box.

To show the advantages of using a grating, we compare, on Figs. 2(a) and 2(c), the emission spectra at a grazing angle for a grating surface and in the specular direction for a smooth surface for normal and oblique incidence, θ_i=0° and 30°, respectively. These angles are chosen because harmonic emission is mostly in the specular direction for smooth targets but more at grazing angles for gratings. We can see how the grating affects the harmonic emission: harmonics having a wavelength $\lambda_r=\lambda_L/4n$ when θ_i=0° and $\lambda_r=\lambda_L/8n$ when θ_i=30° are strongly enhanced, n being an integer. For example, the 20th (θ_i=0°) and the 24th (θ_i=30°) harmonic both have an intensity around $5\times10^{-4}I_L$. Moreover, the harmonics are emitted nearly along the surface, in a narrow lobe, as can be seen on Figs. 2(b) and 2(d), suggesting that the emission is fairly coherent. For normal incidence, we varied the grating periodicity, making $a=\lambda_L/3$ and $\lambda_L/8$, and the results were analogous: the harmonics of the grating periodicity were strongly amplified along the surface. These harmonics are more than one order of magnitude above the corresponding intensities for a smooth target up to harmonic 31 and even beyond. For example, when θ_i=30° and α=0° (not shown), we obtained normalized intensities of 2×10^{-4} for harmonic 31 and 2×10^{-5} for harmonic 40.

This harmonic emission is due to the violent electron dynamics at the protuberances illustrated by the zooms on the electron density in space (x,y) on Fig. 3(a) and in phase space $(x,v_x/c=\gamma\beta_x)$ on Fig. 3(b), where $\gamma=1/\sqrt{1-\beta^2}$. We see relativistic electron bunches coming from the protuberances (every half laser cycle) and traveling mostly along the surface. Before, at its maximum, the ponderomotive force is strong enough to push most of the electrons of a protuberance inwards, and as it weakens, the space charge expels them outwards. Then, the laser electric field pushes them along the surface, while the space-charge field and the ponderomotive force, which becomes gradually stronger, keep them near the surface, and then push them back into the plasma at high speed.

It should be mentioned that, at normal incidence on smooth surfaces, the surface oscillation due to the ponderomotive force may give rise to a two-dimensional (2D) surface wave, leading to a rippling of the plasma surface [18]. This mechanism is unlikely to happen here because the

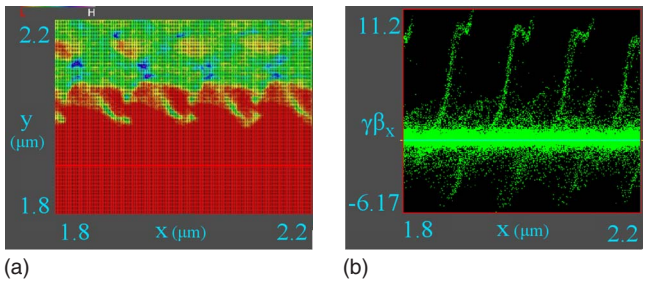

FIG. 3. (Color online) (a) Zooms on electron density and (b) phase space $(x,\gamma\beta_x)$ at 1.5 fs before the peak of the pulse. The numbers indicate the ranges of x and y in μm and of $\gamma\beta_x$.

charge separation at the protuberances completely modifies the surface dynamics.

We have developed a semianalytic model to better understand the dynamics of this situation, and it allowed us to reproduce the main features of the spectra and angular dependences obtained from the full PIC simulations shown in Figs. 2(a) and 2(b). The laser electric field was approximated as a stationary wave by the Fresnel formula for a step density profile of density $4N_c$ (reduced from $20N_c$ due to relativistic effects [14]), and the laser magnetic field was deduced from Faraday's law. To account for the effect of the motion of the plasma surface driven by the ponderomotive force, we added the analytic form of the field due to the protuberances, plus a space-charge field, uniform in x, both oscillating at twice the laser frequency. By numerically solving the relativistic equations of motion for 100 electrons (with appropriate initial velocities and positions distributions) emanating from one protuberance and following them during half a laser cycle, we saw trajectories resembling those seen on Fig. 3. We then computed the radiation fields [19] emanating from these electrons, using the numerically obtained positions and momenta for each time step, and found a fairly wide angular distribution for the harmonics but with a maximum near 0°, as this relativistic motion is mostly along the surface (contrary to slower ones, accelerated relativistic particles emit a narrow cone of radiation centered on the direction of the velocity [19]). To obtain a spectrum and an angular distribution similar to those seen on Fig. 2(a) and 2(b), we assumed that similar trajectories were repeated 33 times with the protuberances separated by $\lambda_L/4$ (to mimic our $8\lambda_L$ wide grating) and added the signals' fields, taking their phases into account, and indeed, we then saw that harmonics 4, 8, 12,… stood out and that the angular distributions were as narrow as those seen on Fig. 2(b) and centered at 0° (to also see the lobe near 180°, we would have needed to also simulate another laser half-cycle, with the laser field in the opposite direction).

Constructive interference of the emitted waves is the key to the spectra and the angular distributions. As is seen on Fig. 1, for the total optical path difference between two neighboring protuberances to be a multiple of the emitted wavelength requires: $n\lambda_r = |\delta_1 - \delta_2| = a|\sin(\theta_i) - \cos(\alpha)|$. For normal incidence, ($\theta_i = 0°$), and for $\alpha = 0°$ (or 180°), this implies $\lambda_r/a = n$, hence the observation of harmonics $\lambda_r = \lambda_L/4, \lambda_L/8, \lambda_L/12, \ldots$ (as $a = \lambda_L/4$). As there is less emission at angles far from $\alpha = 0°$ or 180°, there is less coherent buildup. This explains the spectrum seen on Fig. 2(a), and the relatively low angular spread around $\alpha = 0°$ and 180° seen on Fig. 2(b). When $\theta_i = 30°$, $\sin(\theta_i) = 1/2$ and we see that it is then wavelengths $\lambda_r = \lambda_L/8, \lambda_L/16, \lambda_L/24, \ldots$ which satisfy the condition if $\alpha = 0$, hence the observation of these harmonics on Fig. 2(c) and the angular dependence seen on Fig. 2(d). The slight discrepancies (maximum emission is at 5–10° instead of 0°; some higher harmonics are at slightly different frequencies) are due to the nonuniformity of the laser beam: when using a laser spot size of 3 μm instead of 1 μm, these differences are reduced and for our semianalytic calculation, as there was no such transverse variation in the driving fields, these discrepancies vanished. We mention also that when the laser is incident at an angle $\theta_i = 60°$, for example, the harmonic efficiency and the coherence are strongly reduced because $\sin(\theta_i)$ is then an irrational number.

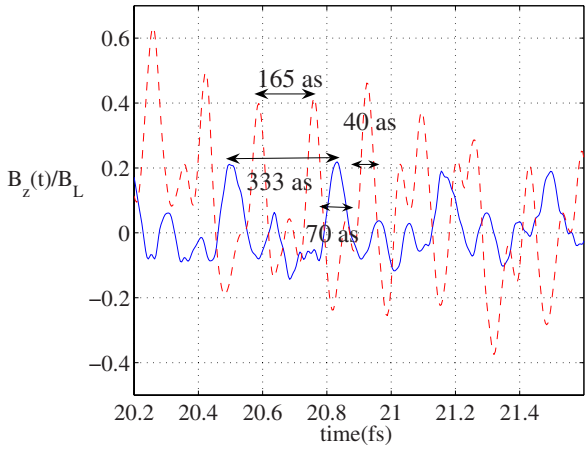

FIG. 4. (Color online) Time dependence of the normalized radiated fields at $\alpha = 10°$ for $\theta_i = 0°$ (solid) and at $\alpha = 5°$ for $\theta_i = 30°$ (broken).

The time dependence of the radiated fields, B_z, shows (Fig. 4) attosecond pulse trains. For $\theta_i = 0°$, we see that a single pulse has a duration $\tau_p \simeq 70$ as $\simeq T_L/19$ ($T_L = \lambda_L/c$), and the delay between pulses is $\tau_d = T_L/4$. For $\theta_i = 30°$, we have an even shorter duration, $\tau_p \simeq 40$ as $\simeq T_L/33$, and the delay between pulses is $\tau_d = T_L/8$.

To study the effect of a higher density, we increased the density from $20N_c$ to 40 and $80N_c$ (these densities are close to those of fully ionized lithium, plastic, and magnesium, respectively), and to keep the same value of the similarity parameter S ($\simeq 4$), we multiplied the intensity (2×10^{20} W/cm^2) by 4 and 16, respectively. The spectra and angular distributions (not shown) and the conversion efficiencies are fairly similar to those seen on Figs. 2(a) and 2(b) for the three cases (as we normalized to the respective incident laser intensities) because the electrons follow similar trajectories in phase space, leading to the same shape of the angular distribution.

We have plotted, for normal incidence, the normalized intensity of harmonic 16 (Fig. 5) in a narrow lobe (170–180°), as a function of S, by varying the intensity, for these three target densities. As many simulations were required for this, they were done with a narrower plasma and a

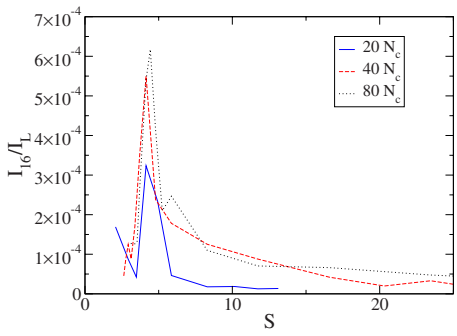

FIG. 5. (Color online) Normalized intensity of harmonic 16 as a function of S at normal incidence for electron densities 20, 40, and $80N_c$.

smaller focal spot ($4\lambda_L$ wide and 1 μm instead of $8\lambda_L$ and 3 μm). There is a clear optimum for harmonic emission near $S=4$. In the case of oblique incidence, we again obtain the same optimum value of S.

This parameter S has a simple physical interpretation when $a_0 \gg 1$: as a_0 is nearly equal to the relativistic mass increase $\gamma=\sqrt{1+a_0^2}$, there is an effective decrease in the plasma frequency $\omega_p'=\sqrt{n_e e^2/\gamma m_e \epsilon_0}$ and we actually have $\omega_p' \simeq \omega_p/\sqrt{a_0}$ [14] so that $S \simeq (\omega_p'/\omega_L)^2$. Therefore $S=4$ corresponds to $\omega_p'=2\omega_L$, implying a resonance with the oscillating motion of the surface at twice the laser frequency due to the ponderomotive force which oscillates between 0 and its maximum value at twice the laser frequency [5,6]. The variation in harmonic emission with S is somewhat different for 40 and $80N_c$ from the $20N_c$ case because, in the latter case, the condition $a_0 \gg 1$ is not so well fulfilled, making similarity theory somewhat less applicable.

This technique of harmonic generation works well if the laser has a very high contrast, otherwise a preplasma is created which changes the laser coupling with the grating. We tried with a $\sin^2$, instead of rectangular, profile for the protuberances, having the same periodicity and grooves' height and the results were similar but less intense, especially the high harmonics. This suggests that even if the grating is altered, it should work for longer pulses.

In conclusion, we have studied the interaction of a relativistic intensity laser beam normally and obliquely incident on an overdense plasma having a gratinglike surface and shown that there is a strongly enhanced emission at harmonics of the grating period, propagating along the target surface in a narrow solid angle. The yield is particularly high if the intensity and density are chosen to make the value of the similarity parameter S close to 4, which is possible with present laser technology [2]. This emission is due essentially to the relativistic motion of electron bunches across the corrugated surface.

The authors thank Professor J. Verboncoeur for his help and guidance on the use of the XOOPIC code and Professors T. W. Johnston, T. Ozaki, F. Vidal, and R. Marjoribanks, and Dr. S. Chelkowski for enlightening discussions. This work was supported by the Ministère de l'Éducation du Québec and the Natural Sciences and Engineering Research Council of Canada.

[1] G. A. Mourou, T. Tajima, and S. V. Bulanov, Rev. Mod. Phys. **78**, 309 (2006).
[2] V. Yanovsky *et al.*, Opt. Express **16**, 2109 (2008).
[3] N. Naumova *et al.*, Phys. Rev. Lett. **93**, 195003 (2004).
[4] G. Kulcsár *et al.*, Phys. Rev. Lett. **84**, 5149 (2000).
[5] R. Lichters, J. Meyer-ter Vehn, and A. Pukhov, Phys. Plasmas **3**, 3425 (1996).
[6] S. V. Bulanov, N. M. Naumova, and F. Pegoraro, Phys. Plasmas **1**, 745 (1994).
[7] B. Dromey *et al.*, Phys. Rev. Lett. **99**, 085001 (2007).
[8] P. Gibbon, Phys. Rev. Lett. **76**, 50 (1996).
[9] N. M. Naumova, J. A. Nees, and G. A. Mourou, Phys. Plasmas **12**, 056707 (2005).
[10] M. M. Murnane *et al.*, Appl. Phys. B: Lasers Opt. **58**, 261 (1994).
[11] S. Kahaly *et al.*, Phys. Rev. Lett. **101**, 145001 (2008).
[12] W.-M. Wang, Z.-M. Sheng, and J. Zhang, Phys. Plasmas **15**, 030702 (2008).
[13] M. Raynaud *et al.*, Phys. Plasmas **14**, 092702 (2007).
[14] J. Kupersztych, M. Raynaud, and C. Riconda, Phys. Plasmas **11**, 1669 (2004).
[15] S. Gordienko and A. Pukhov, Phys. Plasmas **12**, 043109 (2005).
[16] T. Baeva, S. Gordienko, and A. Pukhov, Phys. Rev. E **74**, 046404 (2006).
[17] J. Verboncoeur, A. Langdon, and N. Gladd, Comput. Phys. Commun. **87**, 199 (1995).
[18] A. Macchi *et al.*, Phys. Rev. Lett. **87**, 205004 (2001).
[19] J. D. Jackson, *Classical Electrodynamics* (John Wiley and Sons, New York, 1975).